Journal of Magnetic Resonance 206 (2010) 161–167

Contents lists available at ScienceDirect

Journal of Magnetic Resonance

journal homepage: www.elsevier.com/locate/jmr

Communication

Radiation damping and reciprocity in nuclear magnetic resonance: The replacement of the filling factor ☆

James Tropp [a,*], Mark Van Criekinge [b]

[a] GE Healthcare Technologies, Global Applied Sciences Lab, Fremont, CA, United States
[b] Department of Radiology, University of California San Francisco, Mission Bay Campus, United States

ARTICLE INFO

Article history:
Received 9 March 2010
Revised 20 May 2010
Available online 8 June 2010

Keywords:
Radiation damping
Filling factor
Reciprocity

ABSTRACT

The basic equation describing radiation damping in nuclear magnetic resonance (NMR) is rewritten by means of the reciprocity principle, to remove the dependence of the damping constant upon filling factor – a parameter which is neither uniquely defined for easily measured. The new equation uses instead the transceive efficiency, i.e. the peak amplitude of the radiofrequency B field in laboratory coordinates, divided by the square root of the resistance of the detection coil, for which a simple and direct means of measurement exists. We use the efficiency to define the *intrinsic* damping constant, i.e. that which obtains when both probe and preamplifier are perfectly matched to the system impedance. For *imperfect* matching of the preamp, it is shown that the damping constant varies with electrical distance to the probe, and equations are given and simulations performed, to predict the distance dependence, which (for lossless lines) is periodic modulo a half wavelength. Experimental measurements of the radiation-damped free induction NMR signal of protons in neat water are performed at a static B field strength of 14.1 T; and an intrinsic damping constant measured using the variable line method. For a sample of 5 mm diameter, in an inverse detection probe we measure an intrinsic damping constant of 204 s^{-1}, corresponding to a damping linewidth of 65 Hz for small tip angles. The predicted intrinsic linewidth, based upon three separate measurements of the efficiency, is 52.3 Hz, or 80% of the measured value.

1. Introduction

The damping of the transient signal in pulsed nuclear magnetic resonance (NMR) – as the spins lose energy to the receiver – is called radiation damping; it was first analyzed, a half century ago [1], in the classic work of Bloembergen–Pound (BP), who wrote the Bloch–Kirchhoff equations for the coupling of the nuclear moment to a tuned radiofrequency (RF) detection coil. The resultant damping is essential to the formation of the NMR signal, and occurs in every NMR experiment, although its contribution to the resonance linewidth is often masked by spin relaxation. The theory of damping is therefore central to *any* discussion of sensitivity and detection in NMR.

The subject has had varied applications, including non-linear spin dynamics [2–7], two dimensional spectroscopy [8,9], the design of crafted radiofrequency pulses [10], and the NMR laser [11,12]. Nonetheless, the original theory given by Bloembergen and Pound is still used, even though it no longer reflects a modern view of NMR reception, and contains a problematic figure of merit – the coil filling factor – introduced as a correction to Faraday's law when calculating the signal voltage. The characteristic damping constant then contains the product of the coil filling factor and the resonant Q (or quality factor), which together are taken as a measure of the coil's efficiency [13]. Although the filling factor is neither uniquely defined nor easily measured, its use in the literature of damping has been virtually universal since its introduction. We believe that a good case exists for its replacement, in the context of an updated theory.

We will here show how to rewrite the main damping equation, using the principle of reciprocity, to express the damping constant in terms of a better defined and more readily measured quantity – the transceive efficiency. (The quality factor, although it poses no particular difficulties, will disappear in consequence.) We will also take explicit account of the (often considerable) effects upon the damping constant of variable reflectivity at the preamplifier, which can be substantial, even at input return loss −6 dB. This will lead us to a definition of an *intrinsic* damping constant, i.e. that which is observed when preamplifier and probe are both perfectly matched to a common system impedance – and also to a proposed method for measuring the intrinsic damping, even when the preamp is

☆ Preliminary accounts of this work were presented at meetings of the International Society for Magnetic Resonance in Medicine, in 2004 and 2009, and at the Experimental NMR Conference in 2009.

* Corresponding author. Fax: +1 510 656 4260.
E-mail address: james.tropp@med.ge.com (J. Tropp).

1090-7807/$ - see front matter © 2010 Elsevier Inc. All rights reserved.
doi:10.1016/j.jmr.2010.06.001

matched to some other impedance, which is in fact the common case. We will show data which support the overall correctness and accuracy of our approach.

Following Bloch [14], Bloembergen and Pound wrote the NMR signal voltage by Faraday's law, assuming the flux density to be equal (within a constant) to the transverse magnetization M_t, and obtaining the expression $V = -\eta\mu_0 nAdM_t/dt$ for a long solenoid detection coil of n turns and aperture A. They used the filling factor, defined as $\eta = \int \mathbf{M}\cdot\mathbf{H}\,dV/\mathbf{M}_0\cdot\int \mathbf{H}dV$, (where the H fields are those due to a unit current in the coil) to compensate for the fact that the coil is not fully immersed in sample. In their calculations for the linewidth of water protons, they set $\eta = 1$; and the quantity is often considered to measure the fraction of active antenna volume occupied by sample [15,16]. Other workers have defined the filling factor as the ratio of magnetic field energy in the region occupied by sample, to the total energy of the coil [17,18]; and values less than 0.1 are considered typical.

The modern theory of NMR reception uses the principle of reciprocity [19–22], and treats the magnetization as the source of an oscillatory B field whose time-varying flux is detected through remote coil windows. Saddle coils [19] are widely used, the solenoid having largely disappeared in contemporary practice. Furthermore, reception in biomedical NMR was revolutionized by the development of the array receiver [23], – which posits a collection of simple resonant loops, in close proximity, but electrically decoupled, which receive signal created by an external transmitter producing a homogeneous excitation over the volume of interest. Such situations require a theory in which the signal magnitude and phase are sensitive to the local fields of individual receivers – a condition readily met with application of the reciprocity principle, but less obviously (if at all) tractable by the old canonical theory.

Now admittedly, the reciprocity principle is based upon the assumption of linear media, and its application in magnetic resonance might therefore appear limited to the regime of linear response; but as we shall show in detail, the key formulas for NMR reception depend only upon Faraday's law, and are therefore valid for any preparation of the magnetization, and particularly for any deviation from equilibrium.

2. Theory

Although a general treatment of NMR reception includes circular as well as linear polarization [22,24] of the RF fields, only the latter are of interest here. The principle of reciprocity [22] then gives a simple form for the signal emf:

$$\int \mathbf{E}(r)\cdot d\mathbf{s} = \frac{i\omega_0\mu_0}{I_c}\int \mathbf{H}(r)\cdot\mathbf{M}(r)\,dV \tag{1}$$

where the line integral is taken around the coil winding, the volume integral is over the sample, ω_0 is the Larmor frequency, $\mathbf{E}$ is the electric field due to the vector potential of the magnetization $\mathbf{M}(r)$, and $\mathbf{H}(r)$ is the spatially varying magnetic field produced by peak current I_c in the coil. Although harmonic time dependences are explicitly omitted [25], we have assumed a negative time exponent for Maxwell's equations. Also, although Eq. (1) is commonly called a reciprocity formula, it can be derived without reference to the reciprocity principle (see the Appendix A) by starting from the vector potential $\mathbf{A}$ of a microscopic dipole, $-(\mu_0/4\pi)\mathbf{M}\,dV\times\nabla(1/r)$, transforming the resulting line integral for intercepted flux by means of the Biot-Savart law and vector triple product, and finally integrating over sample volume. Integral transformations of this type, e.g. $\mu_0\int \mathbf{H}(r)\cdot\mathbf{M}(r)\,dV = -\int \mathbf{A}(r)\cdot\mathbf{J}(r)\,dV = -I\Phi$, are common [26], but the application to NMR is aided by the assumption of filamentary currents.

We will assume that the input/output port of the NMR probe is matched to present the system impedance (usually 50 Ω) to the outside world, as is common in analytical NMR systems, and also in many instances, for array antennas in medical imaging. Then for an ensemble of spins, e.g. the protons in a milliliter of water, undergoing Larmor precession following a nutation through the angle ϑ, the equation for balance of the Zeeman energy is [1]:

$$\frac{dE}{dt} = M_0 VB_0\sin\vartheta\frac{d\vartheta}{dt}, \tag{2}$$

assuming M_0 has its thermal equilibrium value, and ignoring relaxation. Since the spins are losing energy, the time derivative of energy in (2) must be negative, and since the magnitudes of the field and magnetization are positive, and the polar angle is assumed to lie between 0 and π, then the time derivative $d\vartheta/dt$ must be negative. That is, the trajectory of the magnetic moment must tend to return it to an orientation parallel to the polarizing field.

Then the available power $P^{(A)}$, deliverable to a matched load from an emf ε with source (i.e. coil) resistance R, is just $\varepsilon^2/4R$; and the total power dissipated in the coil and preamp (source plus load) is twice the available power, per the circuit model of Fig. 1B, with the preamplifier matched (as is the probe) to the system impedance – a condition which will be relaxed subsequently. Also, since the spins undergo many cycles of precession as they gradually lose Zeeman energy, the dissipation must be given as the rms value. The energy balance is now expressed by

$$-\frac{dE}{dt} = 2\times P^{(A)}_{\mathrm{rms}} = \tfrac{1}{2}\frac{\varepsilon^2}{2R} = \frac{\{\omega_0 M_0\sin\vartheta VB_1(1)\}^2}{4R}, \tag{3}$$

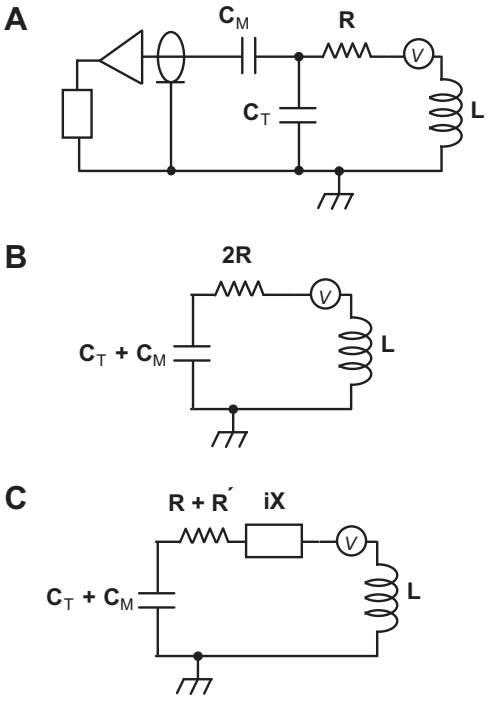

Fig. 1. Circuit model for radiation damping. In 1A, the transduction mesh – the receive coil, its resistance, and capacitors for tuning and impedance matching—couples through a section of transmission line to the preamp. The drive voltage is the emf from precession of the nuclear magnetization. In 1B, on the assumption of perfect matching to the system impedance at both probe and preamp, the load presented by the preamp is transformed to its series equivalent inside the transduction mesh. For the stipulated correct matching, this effectively doubles the resistance in the coil, as reflected the halving of the source-loaded quality (or Q) factor, relative to the unloaded. The summation of tune and match capacitance is an approximation valid for high Q, and therefore applicable to the present work. In 1C, the matching at the probe is assumed perfect, but that at the preamp may deviate from the system impedance. This changes the equivalent circuit of the transduction mesh, causing a variable resistance R' and a variable reactance iX to appear as series elements.

where the peak emf comes from (1), and the factor 1/2 is separated out to emphasize the root mean square value of the power. Also $B_1(1)$ is the peak value in the *laboratory frame* of the radiofrequency B field (assumed uniform over the sample volume V) produced by unit current in the coil, and R is the coil resistance, including the effects of coupling to the NMR sample, but excluding the coupling to the load resistance presented by the receiver.

In the approximation of small nutation angles, this leads directly to the damping equation $d\vartheta/dt = -k\vartheta$, with the damping constant given by $k = \gamma\omega_0 V M_0 \zeta^2/4$, where we introduce the transceive efficiency [27]

$$\zeta = B_1(1)/\sqrt{R} = B_1(I_0)/\sqrt{2P}, \tag{4}$$

with P denoting the rms radiofrequency power absorbed by the probe. The damping equation for arbitrary tip angle ϑ is also easily solved, to yield the familiar result of BP, but with the modified damping constant: $\tan\vartheta/2 = \exp(-kt)$. Furthermore, although we have based our derivation upon energy balance, the same result may be gotten from a torque equation, with the correct sign of the damping emf (for steady state) obtainable directly from the reciprocity principle. We call this value of k, obtained for conditions of perfect matching of all components to the system impedance, the *intrinsic damping constant*. All of our experimental work is performed under conditions of small nutations, in which case the damping lineshape is Lorentzian.

We may also treat case of the preamplifier not matched to the system impedance, and therefore presenting a partially reflective (rather than absorptive) load to the probe. Refer to the circuit model of Fig. 1C. In this case the energy balance Eq. (3) becomes:

$$-\frac{dE}{dt} = \frac{\alpha\{\omega_0 M_0 \sin\vartheta V B_1(1)\}^2}{4R}, \tag{5}$$

where we introduce the dissipation scaling factor α, whose values lie between zero and two, depending upon the coupled resistance R' and reactance iX, which in turn depend upon the impedance mis-match at the preamplifier and the transformation induced by the transmission line (cf Fig. 1C). Then it is easily seen that the new damping constant (denoted by a prime), is just α times the intrinsic damping constant: $k' = \alpha k$. Trivially, the damping linewidth is just k'/π.

With reference to Fig. 1, α clearly must equal $2R/(R+R')$, at its extrema, where the input reflection coefficient at the coil-matching reference plane lies on the meridian line of the Smith Chart. Its values may be estimated or calculated numerically, depending whether or not one has exact knowledge of the probe circuit; but its upper and lower limits are established by intuition or inspection. When R' and iX are both zero (e.g. an infinitely resistive preamp at distance of quarter wave) then the probe tuning (for a moderately high Q factor) is virtually undisturbed, and the total dissipation approaches an upper limit of four times the available power $P^{(A)}$, or twice that of Eq. (3); ergo the value of α is bounded from above by two. In the opposite case, of very large R' and/or iX, the matching mesh is essentially open circuited, which causes (at moderate to high Q values) a significant detuning of the probe. The exact value of dissipation cannot then be known without calculation, but it must always be positive (even though small) and the scale factor is therefore bounded from below by zero.

In Fig. 2A are shown the results of a numerical simulation for the model probe of Fig. 1, with an inductance of 100 nH, and a resistance of 1 Ω, giving α as a function of line length between preamp and probe, for varying degrees of impedance mis-match at the preamp. (Matching of the probe is assumed near-perfect throughout; details of the calculation are found in the Appendix A.) For the preamp very well matched (return loss >50 dB) α assumes the constant value of 1.0, (we assume a lossless line for simplicity.) For

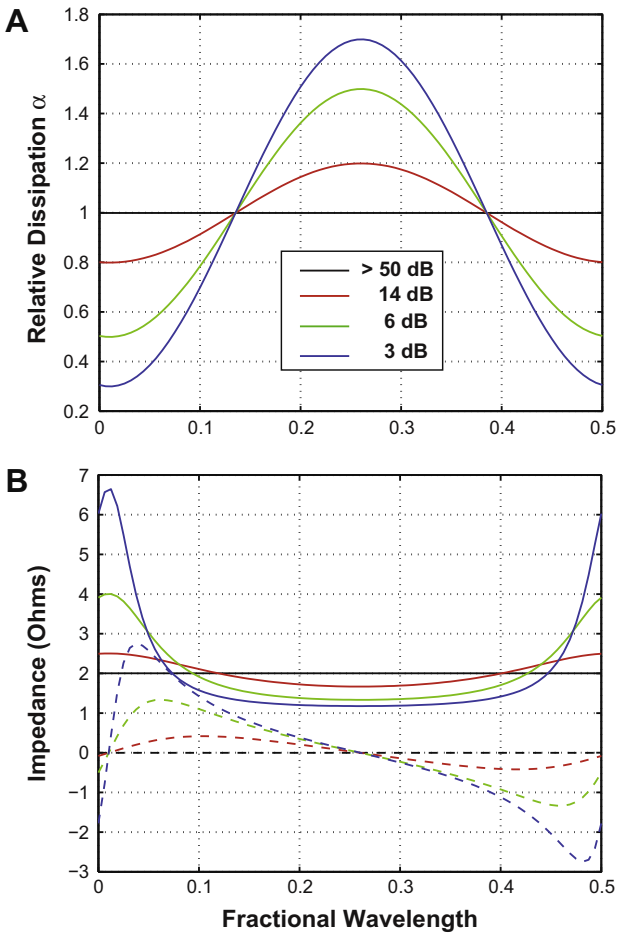

Fig. 2. Results of circuit calculations as described in the text and Appendix A. Above (A), the dissipation scaling factor α, as a function of line length between preamplifier and probe, for various values of the preamplifier return loss ($-20\log_{10}|r|$), per the color key. Below (B), the solid lines give the total resistance (intrinsic plus coupled, i.e. $R + R'$, in Fig. 1C). The dashed lines give the coupled reactive impedances (iX, cf Fig. 1C). Coupled into the probe circuit, per the circuit model of Fig. 1C. The black lines give in both instances the result for perfect matching of both preamp and probe. Note that the dissipation scaling assumes its value for intrinsic damping, at two points, separated by a quarter wave, regardless of the preamp mis-match.

moderately good matching, i.e. return loss of −14 dB, the possible deviations are about ±20%; for −6 dB, ±45%, and so on. The value of α is not usually known apriori, so that the scaling of the damping constant is uncertain in any given measurement. Note in any case the sinusoidal variation of α, which is a direct consequence of the sinusoidal variation of $1/R'$ (cf Appendix A.)

The curves show that, irrespective of mis-match, α assumes unit value repeatedly, at intervals of a quarter wave, and furthermore that the extrema of the deviations are symmetric about unity. (The results are unchanged if the tank circuit is balanced by distributing the tune capacitance.) This immediately suggests a method for measuring the intrinsic damping constant: that is, insertion of a series of calibrated transmission line sections, to vary the line length in small increments over a half wave range. Once the maximum and minimum values of the damping are found (separated by a quarter wave), the intrinsic value is just their average.

While the power calculations for α have been done from Kirchhoff's equation, a simplified version is also possible, using the equivalent single mesh impedance $R + R' + iX$, of Fig. 1C. This impedance, interesting in itself, is calculated by a continued fraction expansion (per the Appendix A), and the results are shown

in Fig. 2B. The coupled resistance is obtained from the plot by subtracting a value of 1.0, which is the assumed value of the probe's own resistance. Then the power calculation may be done by Ohm's law inside the transformed reception mesh of the coil (taking proper account of course of the coupled reactance and noting the coil's own inductance is canceled by the combined tuning and matching capacitance.) The resultant curves (not shown) match those given in Fig. 2A. (The slight displacement in Fig. 2B, i.e. of the maximum resistance for zero separation is straightforwardly visualized as an asymmetry in the Smith chart trajectories for the matching schemes.)

The experiments we shall describe were performed on an NMR scanner operating at 14.1 T (i.e. at a Larmor frequency of 600 MHz for protons), with a sample of neat water in a 5 mm NMR tube, filled to the height of the coil window (1.6 cm). With the efficiency calculated from a nutation of $\pi/2$ in 6.8 μs with 21.4 W pulse power delivered to the probe, we obtain an intrinsic damping constant $k = 171\ s^{-1}$, corresponding to a predicted intrinsic damping linewidth of 54.4 Hz. Pulse power measurements on two other occasions gave the predicted intrinsic linewidth as 57.4 Hz and 45.0 Hz. The average of the three is 52.3 Hz; if the lowest value of 45 Hz is discarded as spurious, the average becomes 54.9 Hz.

3. Results and discussion

We have provisionally measured the intrinsic radiation damping constant, for protons in neat water at 14.1 T, by comparing linewidths of signals acquired with and without detuning of the probe [28], and by varying the electrical distance between preamp and probe, by means of an inserted section of trombone (i.e. variable length) transmission line. Practical details are given in the experimental section. Fig. 3A gives the time course of the free induction decay signals, *without* the trombone section, for the detuned probe above, and the tuned below, in the regime of small nutations, ($\vartheta << \pi/2$). The visual impression is that of a radical difference in damping constant between the two. In Fig. 3B, we superpose the spectroscopic lines resulting from Fourier transformation of the free induction signals. The measured full widths at half height (determined by the spectrometer software) were (in this instance) 44.85 Hz with correct tuning of the probe, and 0.97 Hz with the probe detuned.

In Fig. 4 we present measurements of the damping constant as a function of the length of the inserted trombone section. The insertion loss of the preamp was measured on different occasions to lie between −4.9 and −6.6 dB so that 6 dB line of Fig. 2A gives a reasonable guide for expectation. We plot damping linewidth k'/π versus fractional wavelength, which, in accordance with Fig. 2 and the Appendix A, is fit with a function of the form:

$$k'/\pi = A\sin(2\gamma l - \delta) + k/\pi \tag{6}$$

where the constant A scales with the preamp insertion loss, γ is the propagation constant (assumed lossless), l is the extension of the trombone line in fractions of a wavelength, δ is an empirical offset factor, and the k/π is the intrinsic damping linewidth, for which we obtain the value 65 Hz. The average predicted value (vide supra) of 52.3 Hz is 80% of this value, which is reasonable agreement, if not excellent. The general close agreement of the fit and measured data confirm our basic prediction concerning the variation of the linewidth, even though the measured excursions of linewidth are smaller than the predicted values of Fig. 2. The return loss of the probe was about −30 dB.

Still, reasonable numbers can be gotten with a filling factor. In Fig. 5, for example, we show flux contours for a representative model of an NMR probe with a saddle coil for which we numerically estimate $\eta = 0.073$, with a sample of 5 mm diameter, based

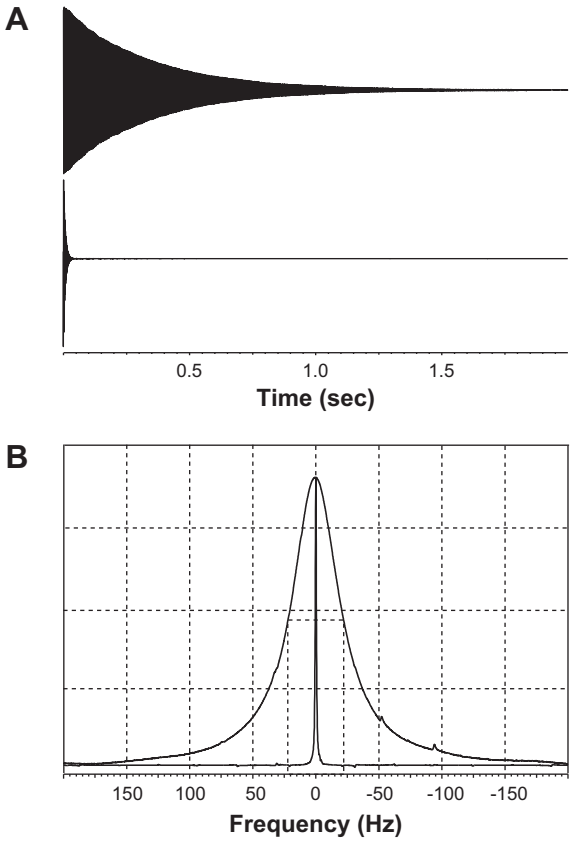

Fig. 3. Results of a representative damping experiment, performed with small nutations ($\ll\pi/2$) as described in the text. In 2A are shown the proton free induction signals of a neat water sample, at 14.1 T (600 MHz), with the NMR probe detuned (above) and correctly tuned (below). The severe condition of damping with the tuned coil is qualitatively visualized. The signal amplitudes are artificially equalized; in fact that from the tuned coil is much larger. In 2B are shown the corresponding spectroscopic lines after Fourier transformation of the free induction signals, overlaid one upon the other, also with artificial equalization of the amplitudes. The full linewidths at the peak half height, determined by the spectrometer software, are 0.98 Hz and 44.85 Hz, giving a damping contribution of about 44 Hz. An inset in the grid allows the damped linewidth to be read approximately from the figure. The small sidebands may be due to phase modulation caused by the spinning of the sample. Some small modulation at 60 Hz may be present.

upon the partition of magnetic energies. Use of this filling factor in the BP formula, with the measured Q value (equal to 225 with source loading), predicts a proton linewidth of 40 Hz, which is 60% of the measured intrinsic damping. (With a filling factor of unity as assumed by BP the result is about 550 Hz.)

But the larger question is, what constitutes the proper definition of filling factor? The common formula, using the partition of energy between filled and empty regions, emerges from a simple treatment of a partially filled inductor in the perturbation limit [29] $L = \mu_0(1+\eta\chi)\int \mathbf{H}(r)\cdot\mathbf{H}(r)\,dV$, with η given by the ratio of energy integrals, over the volume occupied by the load, and over all space. This has also been used for microwave cavities in electron spin resonance; and Feher [30] has given a detailed justification, based upon a detection circuit in which a microwave bridge is unbalanced by an impedance change at resonance, causing in turn a change in reflected power or VSWR. We are unaware however, of a parallel justification for inductive detection, notwithstanding the use of a modified energy-based filling factor in a careful demonstration [31] of radiation damping in bird-cage resonators.

In contrast, the filling factor defined by Bloembergen–Pound is specialized for inductive detection (with solenoid coils), and the integrals are in fact *not* energy integrals, particularly in the case

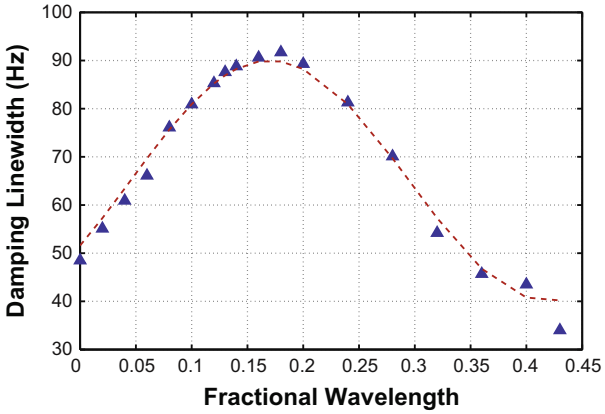

Fig. 4. Results of the damping experiment with variable (trombone) line, as described in the text. The measured linewidth (triangles) is plotted against the electrical extension of the trombone. The dotted line is the fit to Eq. (6) of the text, which yields a value of 65 Hz for the intrinsic damping constant. The data points up to and including 0.4 λ were acquired in a single set up. The final point, inserted at 0.43 λ, is the minimum value observed in all experiments, and is therefore placed a quarter wave away from the maximum at 0.18 λ. Therefore the total plot comprises data merged from two separate set-ups, although strongly weighted towards one of them. The data shown here were recorded without spinning. The linewidth of the sample with detuning was 3.0 Hz, which was subtracted from all of the raw linewidths.

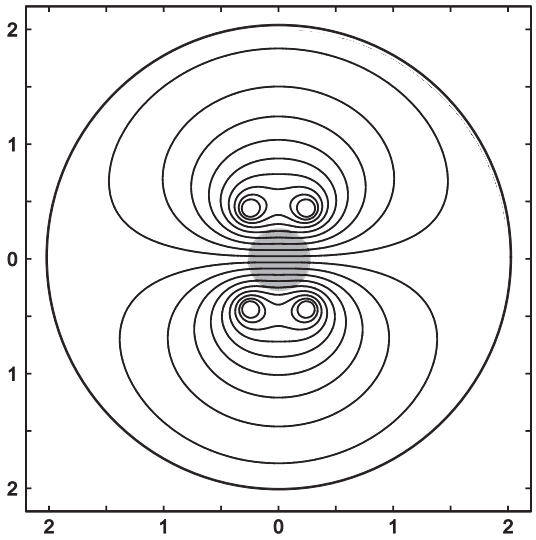

Fig. 5. Two-dimensional model of NMR probe with flux contours of shielded saddle coil for estimation of the filling factor by energy partition, per the text. Axes labeled in cm. A slice is shown perpendicular to the long axis. The saddle coil windows are placed on a bolt circle of 1 cm diameter, have angular aperture of $2\pi/3$ and angular separation of $\pi/3$. The coil assembly sits inside a conductive shield of radius 2 cm, and the coil windings are assumed round, with 0.1 mm radius. The sample, shown in gray highlight is of 5 mm diameter. The flux calculations are done by conformal mapping, as described in the text.

of separate coils for transmission and reception. (A more recent treatment of the filling factor in pulsed electron resonance [32] is also close to that of BP.) Furthermore, the Zeeman energy balance equation in BP leads to the correct damping equation only with the stipulation of a filling factor defined as a ratio of volumes, not energies or voltages, and this interpretation (as noted) is also widely accepted. Therefore a case may be made for each of three separate definitions – as a ratio of voltages, of energies, or of volumes – each with factors to recommend it.

Another question is that of the homogeneity of the RF field. The damping constant has been given here in simplified form, assuming a uniform B_1 field in the reception coil, and a uniform tip angle for magnetization. The net emf for an arbitrary distribution of initial tip angles and local RF field strengths, is given directly by Eq. (1), including the case of separate coils for excitation and reception [22]. However, a solution of the general damping problem with inhomogeneities of RF can only be given numerically, as illustrated in a recent study of damping in toroidal coils [33], in which the accuracy of a calculated filling factor was also considered to be uncertain. We have in any case made a rough measurement of the RF homogeneity in the axial direction, by performing a one dimensional image of a long water sample in the coil. The resultant field plot is given in Fig. 6. We estimate a standard deviation from the mean of 11%, from which we conclude that nearly 90% of the spins in the sample experience the same RF strength. This deviation may account partly for the discrepancy between the measured and calculated damping constant; but confirmation of this point would require detailed simulation with the Bloch equations.

Parenthetically, the reflectivity of the preamp is also of interest, since more reflective devices give weaker damping; also, highly reflective preamplifiers are commonly used in array receivers for medical imaging, to improve decoupling between array elements. However, the great advantage of an absorptive preamp lies in its stability, particularly since the input is derived from an antenna with a sharp resonance, on either side of which the impedance swiftly becomes reactive; under such conditions, a reflective preamp is strongly prone to oscillate.

Finally there is the question of measuring η. Doty and co-workers have given an elegant method [18] using the shift of resonant frequencies upon introduction of a conductive sphere in the active antenna volume. This cannot, however, be considered routine, as it requires a specialized fixture, and detailed knowledge of the coil geometry, to enable placement of the sphere in a region of zero electric energy (inasmuch as that may be found).

The transceive efficiency, on the other hand, is unambiguously defined, and readily measured. It is also in fact a *local* rather than a *global* figure of merit, so that, in case of non-uniform fields, a distribution of values may be determined, using one of the many imaging methods (now widely available on laboratory spectrometers as well as medical scanners) to map the strength of the radio-frequency B_1 field. This is crucial for array receivers, in which the signals received from different points in space vary strongly in both magnitude and phase [23]. But in the common case of a homogeneous B_1 field, the determination of the efficiency still re-

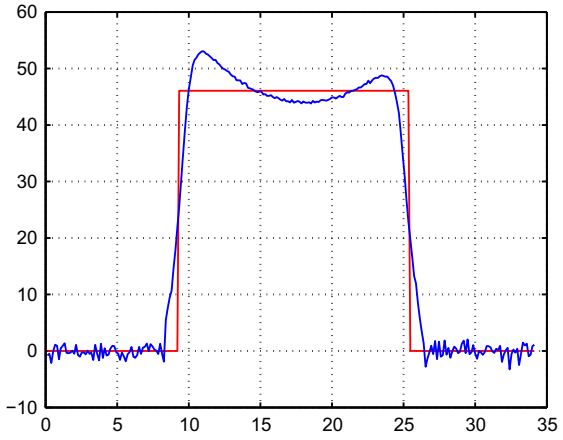

Fig. 6. B_1 field map of the probe from a one dimensional small angle gradient echo image along the cylindrical axis of the probe. The field map (in blue) is in arbitrary units, and was generated from the image by taking the square root of each image point. The horizontal axis is approximate, and is given in mm, based upon the known vertical height of the probe window. The red line is a fit to a top-hat profile of perfect uniformity.

quires only routine measurements of pulsewidth and RF power, without the need of introducing a sensor (often by blind reckoning) into the midst of the radiofrequency detector.

Taken together, we believe these arguments align in favor of the transceive efficiency as a figure of merit for the performance of NMR probes, and as a replacement for the (still) widely used product of filling factor the resonator Q, in future discussions radiation damping. A step in this direction has been taken by Wald and coworkers, who use a parameter they call the transmit efficiency (B_1 per unit current) to calculate the radiation damping field in a feedback system [34]. Our recommendation of course excludes the use of the filling factor concept that may be made in discussing nature and origin of the free induction decay itself [35].

4. Methodology

4.1. Measurement procedures

Spectra were recorded on a narrow-bore Varian INOVA 14.1 T NMR spectrometer, in the Structural NMR Laboratory at the University of California San Francisco, Mission Bay Campus, using the proton channel of the manufacturer's triple-tuned ^{13}C, ^{15}N, ^{1}H 5 mm inverse detection probe, fitted with a z axis gradient set, which was used for shimming. All experiments were a single pulse and acquire, following some minutes of equilibration for the sample to relax and come to temperature, which was set to 25 °C. For the damped experiments, the radiofrequency pulse width was 1.0 μs, for the undamped 1 μs. The sweep width was 10 kHz, with a digital resolution of 0.1 Hz per point, zero filled to 0.05 Hz per point prior to Fourier transformation. The tuning of the probe was determined by measuring the forward scattering parameter S_{11} with an Agilent 5071 network analyzer, with reference planes and cable losses corrected using the manufacturer's electronic calibration fixture. The starting return loss of the probe was adjusted −30 dB at 599.89 MHz, and the quality factor Q was then measured 3 dB bandwidth points, giving the value 225 at critical coupling to the line.

Detuning of the probe (for measuring the undamped linewidth) was monitored on the network analyzer. Typically the resonance was tuned 20–30 MHz away from the Larmor frequency, and then de-matched, resulting in a typical return loss of about −1 dB at Larmor.

Prior to NMR measurements, the transmitter power delivered to the probe was measured with an Agilent E 4443 spectrum analyzer, using calibrated cables and attenuators. The analyzer was set up with large bandwidth, zero sweep, and video trigger. The measured insertion loss of the test gear was typically −34.4 dB; sometimes an extra 10 or 20 dB attenuator was included. A representative analyzer reading with the scanner transmitter gain at its maximum and 40.6 dB attenuation (including cables) was 2.5 dBm, corresponding to a power of 20.5 W. No attempt to estimate the transmission cable losses inside the probe.

The probe efficiency was then determined using a scanner software routine to measure the duration τ of a 2π nutation, from which the familiar equation $2\pi = \frac{1}{2}\gamma B_1 \tau$ gives the strength of B_1 in the laboratory frame. Since this is known to sometimes give spurious results for strongly damping samples, a highly deuterated sample was substituted. This caused a small change in the input match, typically remeasured at −16 dB return loss, down from −30 dB with the neat water sample. No attempt was made to retune the probe, or to correct the linewidth calculations for the difference in reflected power, which would amount to about 2.5% of the available power. The efficiency was calculated from Eq. (4) above, using the power, measured as described above.

Measurement of the preamp input return loss was performed on different occasions with preamp *in situ* and also removed from the scanner. The reference plane for the scattering parameter S_{11} was set at the measurement cable's end, using the network analyzer's electronic calibration module. Prior to calibration, the input sweep power was decreased from 0 dBm to −20 dBm, to avoid gain compression.

The wavelength at 600 MHz inside the trombone line (General Radio 874 LK 20 L, air articulated variable length coaxial line) was verified to have its free space value of 0.5 m by measuring the electrical length as determined by S_{11}. For damping measurements, the trombone was connected between probe and preamp, and its spatial increments measured with a plastic ruler, by an operator seated under the magnet, while another at the spectrometer console oversaw the NMR measurements. Linewidths were determined by the spectrometer software.

The sample was distilled, de-ionized, micropore-filtered water in a standard 5 mm NMR tube, with no deuterium added for lock. The scanner's variable temperature unit was set to 25 °C. Although the bulk of the data, including all those shown in Fig. 4, were collected without sample spinning, the spinner was occasionally used, e.g. for the spectra in Fig. 3, and the spinning rate, although not recorded, was probably about 26 Hz.

4.2. Calculations

The damping linewidth was calculated from Eq. using the formula for the sample dipole moment $\mu = M_0 V = 1/2\gamma\hbar N M_w (\tanh \hbar\omega/2kT)\pi r^2 h_w \times 10^{-3}$, where N is the Avogadro number, M_w is the molarity of water protons (110), r is the inside radius (in cm) of a 5 mm Wilmad NMR tube determined from the manufacturers outer diameter and wall thickness (0.43 mm) and h_w is the height of the probe window, 1.6 cm. The value at $T = 298$ K is 9.73×10^{-9}. The multiplicative factor of 10^{-3} converts the volume to liters, as required by the use of molarity.

Calculations of the flux contours (iso-contours of vector potential) for the filling factor were done by conformal mapping [36], and the results numerically evaluated in Matlab™ scripts written for the occasion. The magnetic fields were gotten by numerical differentiation.

All circuit calculations were also done in Matlab™, using custom scripts, as noted. The underlying equations are given in the Appendix A.

Acknowledgments

This work was supported by General Electric Healthcare Technologies. The authors thank Dr. Kayvan Keshari and Dr. Hikari Yoshihara for help with the spectroscopic and imaging measurements, and also Dr. Carl Carter and Arthur Brooke for helpful discussions. The fuller investigation of the relation between damping and preamp reflectivity was prompted in part by a referee's comments.

Appendix A

For the convenience of the reader, we give here the fuller derivations of some equations occurring in the text. For Eq. (1), we write the time derivative of vector potential due to time varying magnetization in a small volume dV' located at r':

$$\dot{\mathbf{A}}(r) = (i\omega\mu_0/4\pi)\mathbf{M}(r')\,dV' \times \nabla(1/r - r') \tag{A1}$$

where we use negative time exponent for all electromagnetic quantities. We then proceed to Faraday's law for the magnetization in the small volume:

$$\oint \dot{\mathbf{A}} \cdot d\mathbf{s} = (i\omega\mu_0/4\pi)\,dV' \oint \mathbf{M}(r') \times \nabla(1/r - r') \cdot d\mathbf{s}, \tag{A2}$$

where the line integral is taken about the coil perimeter, for which we assume (for simplicity) a filamentary current. The observation point r lies on the integration path. Noting that the vector potential is related to the electric field by $\dot{\mathbf{A}} = -\mathbf{E}$, plus rearrangement of the vector triple product and application of the Biot-Savart law, followed by integration over the primed volume, yields Eq. (1) of the main text directly. No stipulation is placed upon the state of the magnetization, so that the equation stands without reference to the reciprocity principle or the linearity (or not) of the medium. Since the factor $(1/r - r')$ is essentially the quasistatic Green's function, we may replace it with a more general electromagnetic Green's function $G(r, r')$ and achieve somewhat greater generality. A specific example of the free space Green's function is given by Insko et al. [37], although their calculation assumes a homogeneous medium throughout all space.

The most direct means of calculating the dissipation scale factor α in Fig. 2A is via the Kirchhoff mesh equations, starting the transformed impedance of the preamp as seen by the probe: $Z' = Z_0(1 + \rho\exp(2i\gamma l)/(1 - \rho\exp(2i\gamma l)$, where the reflection coefficient ρ is measured directly at the preamp input, and l is the length of transmission line and γ is the propagation constant, which we assume lossless for simplicity. Then, the Fourier-transformed Kirchhoff mesh equations describing the circuit model of Fig. 1A are

$$\begin{bmatrix} i\omega L + 1/i\omega C + R & -1/i\omega C \\ -1/i\omega C & 1/i\omega C + 1/i\omega C_M + Z' \end{bmatrix} \begin{bmatrix} I_1 \\ I_2 \end{bmatrix} = \begin{bmatrix} 1 \\ 0 \end{bmatrix} \tag{A3}$$

where we have assumed a unit drive voltage from the sample. Then the total dissipation is $P = |I_1|^2 R + |I_2|^2 \mathrm{Re}(Z')$, where we have assumed, the conversion to rms values. Note that $\mathrm{Re}(Z') = R' = Z_0(1 - |\rho|^2)/(1 - 2\rho\cos 2\gamma l + \rho^2)$, so that the inverse coupled resistance has a sinusoidal dependence on the doubled electrical distance. This explains the sinusoidal form of the curves in Fig. 2A. (The starting value at zero distance corresponds to maximum resistance, which implies an arbitrary offset, of no fundamental importance, in the application to experimental data.)

We also calculate the transformed impedance values in Fig. 1C, by a continued fraction:

$$R + R' + iX = (i\omega L + R) + \cfrac{1}{i\omega C + \cfrac{1}{Z + \frac{1}{i\omega C_M}}}. \tag{A4}$$

References

[1] N. Bloembergen, R.V. Pound, Phys. Rev. 95 (1954) 8.
[2] S. Bloom, J. Appl. Phys. 28 (1957) 800.
[3] A. Szöke, S. Meiboom, Phys. Rev. 113 (1959) 585.
[4] V.I. Yukalov, Phys. Rev. Lett. 75 (1995) 3000.
[5] W.S. Warren, S.L. Hames, J.L. Bates, J. Chem. Phys. 91 (1989) 5895.
[6] M.P. Augustine, S.D. Bush, E.L. Hahn, Chem. Phys. Lett. 322 (2000) 111.
[7] X.-A. Mao, J.-X. Guo, C.-H. Ye, Phys. Rev. B 49 (1994) 15702.
[8] A. Vlassenbroek, J. Jeener, P. Broekaert, J. Chem. Phys. 103 (1995) 5886.
[9] A.G. Sobol, G. Wider, H. Iwai, K. Wüthrich, J. Magn. Reson. 130 (1998) 262.
[10] D.E. Rourke, M.P. Augustine, Phys. Rev. Lett. 84 (2000) 1685.
[11] P. Bösiger, E. Brun, D. Meier, Phys. Rev. A 18 (1978) 671.
[12] B. Derighetti, M. Ravani, R. Stoop, F. Meier, E. Brun, R. Badii, Phys. Rev. Lett. 55 (1985) 1746.
[13] F.D. Doty, The Encyclopedia of NMR, Wiley, New York, 1996. p. 3753 ff.
[14] F. Bloch, Phys. Rev. 70 (1946) 460.
[15] A. Abragam, The Principles of Nuclear Magnetism, Oxford University Press, London, 1961. p. 74 ff.
[16] T. Sleator, E.L. Hahn, C. Hilbert, John Clarke, Phys. Rev. B 36 (1987) 1969.
[17] H.D.W. Hill, R.E. Richards, J. Phys. E Ser. 2 (1968) 977.
[18] F.D. Doty, J.G. Entzminger, C.D. Hauck, J.P. Staab, J. Magn. Reson. 138 (1999) 144.
[19] D.I. Hoult, R.E. Richards, J. Magn. Reson. 24 (1976) 71.
[20] H. Vesselle, R.E. Collin, IEEE Trans. Biomed. Imaging 42 (1995) 497.
[21] R.F. Harrington, A.T. Villeneuve, IRE Trans. Microwave Theory and Technique, MTT6, 308, 1958.
[22] J. Tropp, Phys. Rev. A 74 (2006) 062103.
[23] P.B. Roemer, W.A. Edelstein, C.E. Hayes, S.P. Souza, O.M. Mueller, Magn. Reson. Med. 16 (1990) 192.
[24] D.I. Hoult, C.-N. Chen, V.J. Sank, Magn. Reson. Med. 1 (1984) 339.
[25] L.D. Landau, E.M. Lifshitz, Electrodyamics of Continuous Media, Pergamon, New York, 1960. p. 289 ff.
[26] L.D. Landau, E.M. Lifshitz, ibid, p. 126.
[27] D.I. Hoult, P.C. Lauterbur, J. Magn. Reson. Med. 34 (1979) 425.
[28] A. Abragam, ibid., p. 63 ff.
[29] R.E. Collin, Foundations of Microwave Engineering, IEEE Press–Wiley Interscience, New York, 2000. p. 155.
[30] G. Feher, Bell Syst. Techn. J. 36 (1957) 449.
[31] P. Teh, N. DeZanche, J. Wild, J. Magn. Reson. 185 (2007) 164.
[32] A. Blank, H. Levanon, Spictrochim. Acta (Part A) 58 (2002) 1329.
[33] K.I. Momot, C.S. Johnson Jr, J. Chem. Phys. 115 (2001) 3992.
[34] S.Y. Huang, T. Witzel, L. Wald, Magn. Reson. Med. 60 (2008) 1112.
[35] D.I. Hoult, N.S. Ginsburg, J. Magn. Reson. 148 (2001) 182.
[36] W.R. Smythe, Static and Dynamic Electricity, third ed., McGraw Hill, New York, 1968 (Chapter IV).
[37] E.K. Insko, M.A. Elliott, J.C. Schotland, J.S. Leigh, J. Magn. Reson. 131 (1998) 111.